

Doublet luminescence due to coexistence of excitons and electron-hole plasmas in optically excited $CH_3NH_3PbBr_3$ single crystal

Jie Wang(王杰), Guang-Zhe Ma(马广哲), Lu Cao(曹露), Min Gao(高敏), and Dong Shi(石东)
Citation: Chin. Phys. B, 2022, 31 (**4**): 047104. DOI: 10.1088/1674-1056/ac29b5
Journal homepage: http://cpb.iphy.ac.cn; http://iopscience.iop.org/cpb

What follows is a list of articles you may be interested in

Self-screening of the polarized electric field in wurtzite gallium nitride along [0001] direction

Qiu-Ling Qiu(丘秋凌), Shi-Xu Yang(杨世旭), Qian-Shu Wu(吴千树), Cheng-Lang Li(黎城朗), Qi Zhang(张琦), Jin-Wei Zhang(张津玮), Zhen-Xing Liu(刘振兴), Yuan-Tao Zhang(张源涛), and Yang Liu(刘扬)
Chin. Phys. B, 2022, 31 (**4**): 047103. DOI: 10.1088/1674-1056/ac4746

Tunable electronic properties of GaS-SnS_2 heterostructure by strain and electric field

Da-Hua Ren(任达华), Qiang Li(李强), Kai Qian(钱楷), and Xing-Yi Tan(谭兴毅)
Chin. Phys. B, 2022, 31 (**4**): 047102. DOI: 10.1088/1674-1056/ac3a62

High linearity AlGaN/GaN HEMT with double-V_{th} coupling for millimeter-wave applications

Pengfei Wang(王鹏飞), Minhan Mi(宓珉瀚), Meng Zhang(张濛), Jiejie Zhu(祝杰杰), Yuwei Zhou(周雨威), Jielong Liu(刘捷龙), Sijia Liu(刘思佳), Ling Yang(杨凌), Bin Hou(侯斌), Xiaohua Ma(马晓华), and Yue Hao(郝跃)
Chin. Phys. B, 2022, 31 (**2**): 027103. DOI: 10.1088/1674-1056/ac2b21

Stability, electronic structure, and optical properties of lead-free perovskite monolayer $Cs_3B_2X_9$ (B=Sb, Bi; X=Cl, Br, I) and bilayer vertical heterostructure $Cs_3B_2X_9/Cs_3B_2'X_9$ (B,B'=Sb, Bi; X=Cl, Br, I)

Yaowen Long(龙耀文), Hong Zhang(张红), and Xinlu Cheng(程新路)
Chin. Phys. B, 2022, 31 (**2**): 027102. DOI: 10.1088/1674-1056/ac2e5f

First-principles study on improvement of two-dimensional hole gas concentration and confinement in AlN/GaN superlattices

Huihui He(何慧卉) and Shenyuan Yang(杨身园)
Chin. Phys. B, 2022, 31 (**1**): 017104. DOI: 10.1088/1674-1056/ac00a0

Doublet luminescence due to coexistence of excitons and electron–hole plasmas in optically excited $CH_3NH_3PbBr_3$ single crystal

Jie Wang(王杰)[1], Guang-Zhe Ma(马广哲)[1], Lu Cao(曹露)[1], Min Gao(高敏)[2], and Dong Shi(石东)[1,†]

[1] *School of Optoelectronic Science and Engineering, University of Electronic Science and Technology of China, Chengdu* 610054, *China*
[2] *School of Materials and Energy, University of Electronic Science and Technology of China, Chengdu* 610054, *China*

(Received 21 June 2021; revised manuscript received 30 August 2021; accepted manuscript online 24 September 2021)

Doublet luminescence from hybrid metal trihalide perovskite semiconductors is observed along with materials processing when high-quality single crystals are obtainable. Yet, the underlying physical mechanism remains poorly understood. Here, we report controllable solution-processed crystallization that affords high-quality $CH_3NH_3PbBr_3$ single crystals with atomically flat pristine surfaces. Front-face photoluminescence (PL) shows doublet luminescence components with variable relative intensities depending on the crystal surface conditions. We further find that the low-energy PL component with asymmetric spectral line-shape becomes predominant when the atomically flat crystal surfaces are passivated in the ion-abundant saturated solutions, while poor-quality single crystal with visually rough surface only gives the high-energy PL with symmetric line-shape. The asymmetric spectral line-shape of the low-energy PL matches perfectly with the simulated bandedge emission. Therefore, the low-energy PL component is attributable to the intrinsic bandedge emission from the crystal bulk while the high-energy one to surface-specific emission. Elliott fitting to the absorption data and multi-exponential fitting to the time-resolved photoluminescence traces jointly indicate the coexistence of excitons and electron–hole plasmas in optically excited $CH_3NH_3PbBr_3$ single crystals, thereby catching the physical merit that leads to the occurrence of doublet luminescence.

Keywords: semiconductor, crystal, surface, luminescence

PACS: 71.10.Li, 71.20.Nr, 71.15.Qe **DOI:** 10.1088/1674-1056/ac29b5

1. Introduction

Research interests in metal halide perovskite semiconductors has been rekindled following the breakthroughs in solar-to-electric power conversion efficiencies achieved via the use of the prototypical hybrid methylammonium lead trihalide perovskites, $CH_3NH_3PbX_3$ (X = Br, or I), in photovoltaic cells.[1–3] A couple of solution-processed material processing protocols, including the well matured one-step and sequential spin coating,[4,5] strongly backgrounded the fast development of perovskite photovoltaics in the past decade.[6–9] More recently, while perovskite photovoltaic technologies are approaching the edge of commercialization,[10] other applications of the halide perovskites for lasing,[11,12] light-emitting diodes,[13,14] photodetectors,[15,16] x-ray detectors[17,18] were lightened simultaneously.

Driven by the pursuit for ever-increasing device performances, intensive research efforts were devoted to improved solution-processed materials processing by scientist with diverse academic backgrounds.[19–22] Most remarkable among the advances in material processing was the growth of high-quality single crystals that enabled improved understanding on the optoelectronic superiorities of halide perovskites.[23,24] To the delight of fundamental researchers interested in catching the intrinsic material physics, room-temperature solution-grown $CH_3NH_3PbBr_3$ and $CH_3NH_3PbI_3$ single crystals demonstrated extraordinarily low trap-sate densities that are superior to a wide array of established inorganic semiconductors.[23] Therefore, the extrinsic effects associated with defects, surface roughness and midgap states get largely suppressed when running spectroscopic characterizations.[25–27] Indeed, new optical phenomena shown by high-quality halide perovskite single crystals other than their polycrystalline thin-film counterparts are being observed.[28] One of the most intriguing phenomena is the occurrence of doublet luminescence shown the front-face PL from high-quality single crystals of the most studied prototypical $CH_3NH_3PbBr_3$ and $CH_3NH_3PbI_3$ perovskites.[23,28,29] Although repeatedly observed, the underlying physical mechanism that leads to the occurrence of such doublet PL remains poorly understood. A crystal-clear elucidation on the physical origin of the doublet PL is an outstanding quest, in view of its direct consequence on diverse optoelectronic functionalities.

We were thus motivated to revisited the spectroscopic properties shown by one of the most studied prototypical hybrid metal halide perovskites, $CH_3NH_3PbBr_3$, in its single crystal form. Practically, single-crystal samples with variable surface roughness were prepared and used for spectroscopic

†Corresponding author. E-mail: dshi@uestc.edu.cn
© 2022 Chinese Physical Society and IOP Publishing Ltd

characterizations. By interpreting the spectroscopic data according the established physical theorems in semiconductor optics, we figured out the physical origin of the doublet luminescence, i.e., the coexistence of surface-specific excitons and electron–hole plasma inside the crystal bulk of optically excited $CH_3NH_3PbBr_3$ single crystal.

2. Materials and methods

2.1. Materials

The two $CH_3NH_3PbBr_3$ perovskite precursors, CH_3NH_3Br and $PbBr_2$ were purchased from Xi'an Polymer Light Technology Corp. The solvent, N, N-dimethylformamide (DMF) was purchased from Shanghai Titan Scientific Co., Ltd.

2.2. Methods

2.2.1. Crystallization

Room-temperature slow solvent evaporation from the precursors' solution in DMF yielded high-quality $CH_3NH_3PbBr_3$ single crystals. In particular, $PbBr_2$ and CH_3NH_3Br (1:1 by molar $\sim$ 1.0 M) were dissolved in DMF in screw capped vials, stirred for 3 hours, filtered through a syringe filter ($\text{Ø} = 0.45$ μm), and eventually yields a colorless and transparent solution. Then, the solvent was allowed to evaporated out of the solution phase at room temperature and 1.5 atm in a nitrogen-filled gloved box. The crystallization procedure is schematically shown in Fig. 1(a).

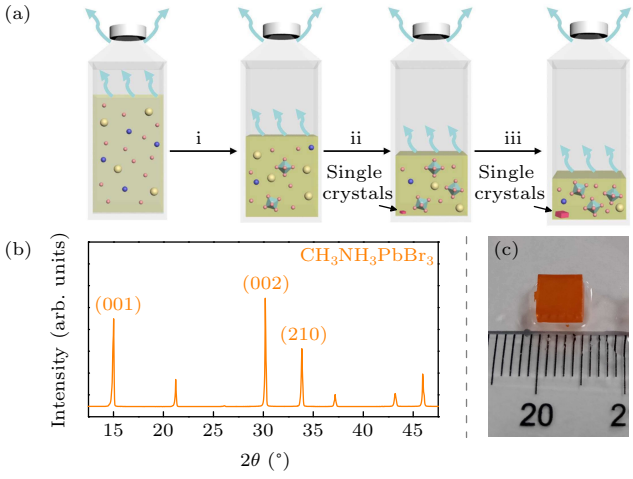


Fig. 1. (a) Schematic diagram of the crystallization processes. Yellow sphere represents $CH_3NH_3^+$, blue sphere represents Pb^{2+}, pink sphere represents Br^-. (b) Experimental powder XRD profile of $CH_3NH_3PbBr_3$ single crystal ground into powders. (c) Photograph of one piece of $CH_3NH_3PbBr_3$ single crystal with $\sim$ 5 mm dimensions.

2.2.2. Structural and spectroscopic characterizations

The phase purity of the as-grown $CH_3NH_3PbBr_3$ single crystals was confirmed by x-ray diffraction (XRD) which can give detailed lattice information. The diffractometer, Maxshima XRD-7000 that equips with the standard Cu-$K\alpha_1$ excitation radiation source and a diffracted beam monochromator, was used. The surface morphologies of the as-grown pristine single crystals were characterized by Asylum MFP-3D atomic force microscopy (AFM). The absorbance of highly transparent $CH_3NH_3PbBr_3$ single crystals was recorded in a transmission mode using Shimadzu UV-2600 spectrometer. The front-face steady-state PL and time-resolved photoluminescence (TRPL) were recorded by FluoTime 300 fluorometer (PicoQuant) equipped with a time-correlated single photon counting (TCSPC) detector. The crystal sample was photoexcited by a picosecond pulsed diode laser (PicoHarp, LDH-D-C-405M, exciting at 400 nm, repetition rate: 0.2 MHz).

3. Results and discussion

Figure 1(a) schemes the crystallization procedure via slow solvent evaporation out of the precursor ($PbBr_2$ and CH_3NH_3Br, 1:1 by molar) solution in DMF. Slow solvent evaporation at room temperature allows for balanced ionic incubation in the solution phase, whereby freely solvated Pb^{2+} and Br^- ions self-assemble into the energetically more stable octahedral corrodinates, $[PbX_6]^{4-}$. Once crystallization starts when both precursors saturates along with solvent evaporation, the solution phase remains invariable in concentration afterwards. This leads to invariable stoichiometric conditions surrounding the enlarging crystal surfaces all around. In this scenario, by gingerly screwing down the cap without causing too much disturbance, freshly incubated perovskite single crystals would be obtained. In the presence of passvation by the constituent ions in the solution, the crystal surface is expected to be characterized by naturally orientated surface dangling bonds.

The crystal phase purity of the room-temperature grown single crystals was confirmed by powder XRD. A random batch of the as-grown single crystals were collected, grinded into powders, and then mounted in the sample holder of the diffractometer. The collected XRD data was shown in Fig. 1(b). Characteristic diffractions at $2\theta = 15.1°$, 30.2°, and 33.8°, which are assigned to the characteristic (001), (002), and (210) planes of the cubic $CH_3NH_3PbBr_3$ single crystal, are observed.[3] All diffractions were precisely assigned to the its well-known room-temperature cubic lattice symmetry, indicating crystal phase purity. Figure 1(c) shows a representative photograph of one piece of the as-grown pristine $CH_3NH_3PbBr_3$ single crystal. Notably, the sharp edges of the regular square shapes nicely reflect its cubic crystal symmetry.

The surface morphologies of freshly grown pristine $CH_3NH_3PbBr_3$ single crystals were characterized by AFM. One best-case top-view morphology showing rather smooth

surface and least density of surface nanoparticles is shown in Fig. 2(a). One moderate-case and one worst-case morphologies showing increased surface roughness are selectively provided in Figs. 2(b) and 2(c), respectively.

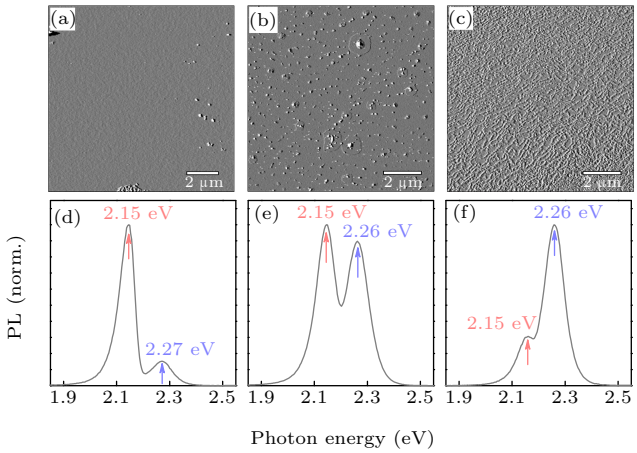


Fig. 2. (a)–(c) Pristine surface morphologies of three $CH_3NH_3PbBr_3$ single-crystal samples viewed under AFM. (d)–(f) Front-face PL spectra corresponding to the crystal surface morphologies shown in (a)–(c), respectively.

When recording the luminescence spectra generated by front-face photoexcitation, the illuminated surface was oriented about 30° from the incident excitation beam. In this way, the incident light got distributed over large surface area and moreover, strong reflection of light entering the emission monochromator was avoided.[31] The collected PL spectra as a function of photon energy with two components were shown in Figs. 2(d)–2(f) for each case. Notably, the high-energy PL component peaks at 2.26 eV and the low-energy one at 2.15 eV. The peak positions of both components remain invariable regardless of their relative intensities. Similar doublet PL was also observed for high-quality $CH_3NH_3PbI_3$ single crystal in previous studies.[28] Interestingly, the high-energy PL component augments dramatically along with increased surface roughness, indicating that the high-energy PL is attributable to surface-specific emission, while the low-energy PL component is attributable to bulk-specific luminescence.

We further found that by having a piece of high-quality single crystal kept in the saturated mother solution that contains abundant constituent ions, the low-energy PL component became significantly augmented over the high-energy one. In this case, a basically mono-peak PL with asymmetric spectral line-shape, as shown in Fig. 3(a), was observed. The mono-component bulk-dominated PL, peaking at 2.15 eV, carries a long PL tail that extends toward lower photon energy. In addition, a full width at half-maximum (FWHM) value, $\Gamma \sim 75$ meV, is determined. In general, every solid has a surface connecting its bulk to the outer world. For the case with a high-quality $CH_3NH_3PbBr_3$ single crystal, an ideal crystal surface is expected to be an atomically flat surface that carries abundant dangling bonds orienting naturally along the lattice axis without causing lattice deviations and subsequent midgap states formation. To maintain the natural orientation of the dangling bonds, passivation — most preferred by the constituent ions from the outer surroundings over the crystal surface — is required.[32,33] Otherwise, structural deviation at the lattice peripheries are inevitable. In our case, the precursor ions in the colorless saturated mother solution help complete the octahedral coordination at the perovskite lattice periphery and thereby suppress structural distortions. The diagram shown in Fig. 3(b) schematically illustrates the passivation effect of the ion-abundant mother solution.

The occurrence of the asymmetric bulk-PL from high-quality $CH_3NH_3PbBr_3$ single crystal is a universal phenomenon as it has been repeatedly observed previously.[23,34] In this regard, the physical mechanism that leads to the occurrence of the asymmetric PL should be, in principle, rooted in the framework of the intrinsic material physics. The direct bandgap nature defines that the radiative recombination within the lattice bulk of $CH_3NH_3PbBr_3$ single crystal is an inverse process of ligth absorption, which can be expressed via the established van Roosbroeck–Shockley relation[35,36]

$$\gamma_{\mathrm{spon}}(E) \propto (n_{\mathrm{R}}(E)E)^2\,\alpha(E)\exp\left(-\frac{E-E_0}{k_{\mathrm{B}}T}\right). \tag{1}$$

In this expression, $\gamma_{\mathrm{spon}}(E)$ represents the spontaneous emission from the bandedge, and its spectral line-shape is, therefore, correlated with the distribution of the electronic density of states (DOS) at the bandedge. One accessible spectroscopic parameter related to the bandedge DOS is the dimensionless steepness factor, σ, the value of which can be directly determined from the absorption edge according to its correlation with the absorption coefficient, $\alpha(E)$, via

$$\alpha(E) = \frac{\alpha_0}{\exp\left(\sigma\dfrac{E_0-E}{k_{\mathrm{B}}T}\right)+1}. \tag{2}$$

In this expression, α and E can be viewed as a constant, k_{B} is the Boltzmann constant, T is the absolute temperature. In practice, $(n_{\mathrm{R}}(E)E)^2$ is also approximated as a constant for simplicity as it does not affect the simulation. Thus, the bandedge emission can be simulated via

$$\gamma_{\mathrm{spon}} \propto \frac{1}{\exp\left(-(\sigma-1)\dfrac{E-E_0}{k_{\mathrm{B}}T}\right)+\exp\left(\dfrac{E-E_0}{k_{\mathrm{B}}T}\right)}. \tag{3}$$

Figures 3(c)–3(e) show the simulated $\gamma_{\mathrm{spon}}(E)$ corresponding to $\sigma = 1.5$, 2.0, and 3.0 respectively. In this scenario, the line-shape of spontaneous emission spectrum is subjected to the value of σ. The slope of $\gamma_{\mathrm{spon}}(E)$ at the high-energy side is determined by $k_{\mathrm{B}}T$, while at the low-energy side it is determined

by $k_BT/(\sigma-1)$. In Fig. 3(c), the slope at low-energy region is smaller than that at high-energy region, therefore, the observed PL spectrum is asymmetric and is characterized by a long tail that extends to lower energies. When $\sigma = 2.0$, the simulated spectrum becomes symmetric as displayed in Fig. 3(d). When increasing σ to 3.0, the simulated spectrum becomes asymmetric again, but it is characterized by a long tail that extends toward higher energies as shown in Fig. 3(e).

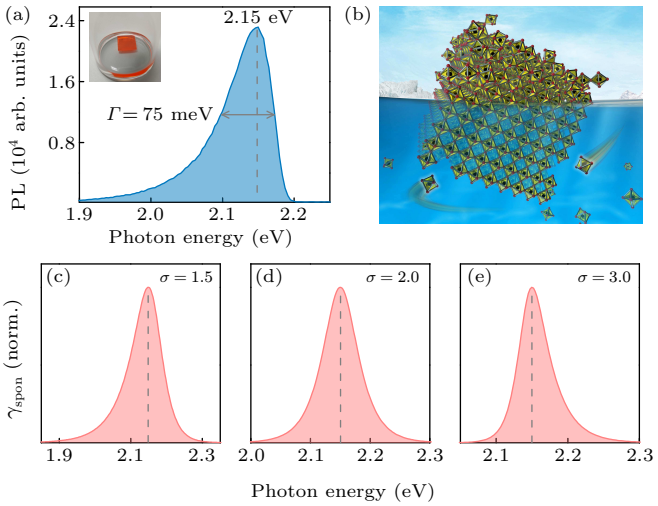


Fig. 3. (a) Asymmetric bulk-specific PL spectrum. The peak position and the FWHM are also reported. Inset: photograph of solution-passivated $CH_3NH_3PbBr_3$ single crystal. (b) Schematic crystal lattice diagram showing largely suppressed deviation when passivated in mother solution. (c)–(e) Simulated bandedge emission spectral line-shapes corresponding to $\sigma = 1.5$, 2.0, and 3.0, respectively.

Based on the above-made discussions, it is clear that the asymmetric bulk luminescence with long tail that extends to lower energies corresponds to σ values between 1.0 and 2.0. This is equivalent to set the values of the Urbach energy, E_U, between 26 meV and 13 meV, according to their relationship, $\sigma = k_BT/E_U$. To confirm this point, we recorded and plotted the logarithmic absorbance against photon energies as shown in Fig. 4(a). Linear fit of the absorption edge yields $E_U = 18$ meV, which corroborates our attribution of the low-energy PL to the intrinsic bulk emission from band-edge states. Although the absorbance of the $CH_3NH_3PbBr_3$ single crystal does not develop into a sharp excitonic peak as that observed in its polycrystalline thin film counterpart, the absorbance data was fitted well with the established Elliott formula.[37,38] The absorbance data along with the Elliott fit were shown in Fig. 4(b). By performing the Elliott fit, contributions to the overall absorption intensity from discrete excitonic states below the gap and band-to-band continuum transitions are decoupled. As shown in Fig. 4(b), absorption by a sum of discrete excitons peaking at $E_X = 2.194$ eV and band gap energy of $E_G = 2.206$ eV were determined. This in turns leads to the determination of the exciton binding energy, $E_B = 12$ meV, according to $E_B = E_G - E_X$. In view of the lower E_B than the room-temperature thermal energy, $k_BT \sim 26$ meV, it is within conceivable expectation that the concentration of excitons in optically excited $CH_3NH_3PbBr_3$ single-crystal bulk should be sufficiently low because of thermal dissociation. Thus, many-body electron–hole (e–h) plasma occurs in the excited phase. On the other hand, it has been repeatedly confirmed that the surface-abundant polycrystalline thin film shows much stronger excitonic feature, and this indicates the co-existence of excitons and e–h plasmas.[39] In a general scenario, the crystal surface behaves as giant lattice defects whereby excitons are apt to adhere.

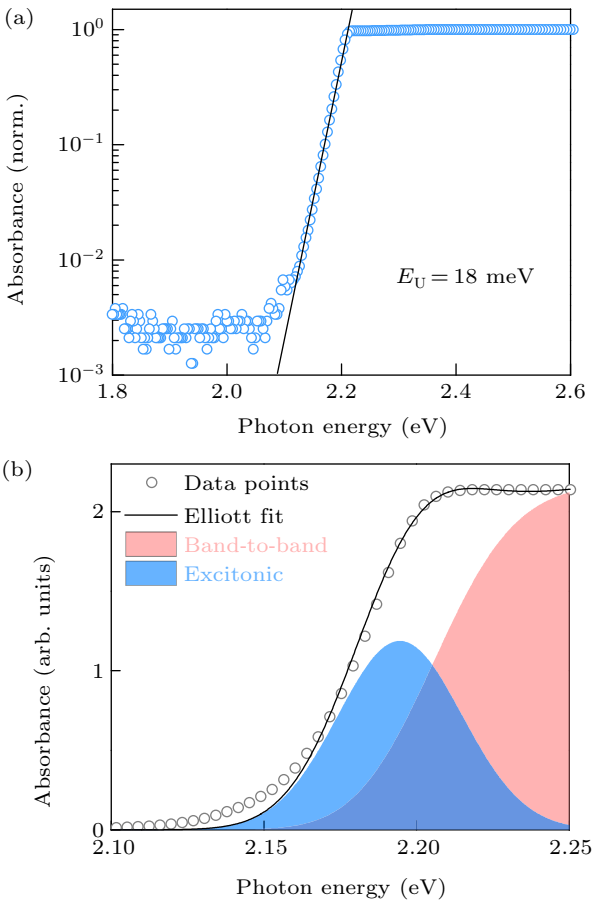


Fig. 4. (a) Normalized logarithm absorbance (blue markers) as a function of photon energy. The black solid line shows the linear fit to the linear region of absorption tail, which yields $E_U = 18$ meV. (b) Absorbance data (grey makers) along with Elliott fit (black solid line) overlaid, the blue and the pink areas reflect the contributions to the absorbance from a sum of discrete excitonic states and band-to-band continuum excitations, respectively.

The co-existence of excitons and e–h plasmas in optically excited $CH_3NH_3PbBr_3$ single crystal was further verified by TRPL measurement. Figure 5 shows the TRPL traces probed under picosecond pulsed photoexcitation at 400 nm. Apparently, the TRPL traces can be fitted well with a bi-exponential function. The bi-exponent fit (blue solid line) was plotted together with the TRPL traces in Fig. 5. The close to unity value of the reduced chi square, χ^2_R, and the symmetric distribution of the standard deviation, δ_k, jointly indicate the accpetalbe goodness-of-fit (GOF). Two lifetime

components, $\tau_1 \sim 2791 \pm 166$ ns representing the lifetime of diffusive e–h plasma and $\tau_2 \sim 179 \pm 81$ ns representing the liftime of surface-specific excitons, were obtained. In addition, the remarkably low intensity ratio of τ_2 further reflects sufficiently low density of excitons in optically excited high-quality $CH_3NH_3PbBr_3$ single crystal.

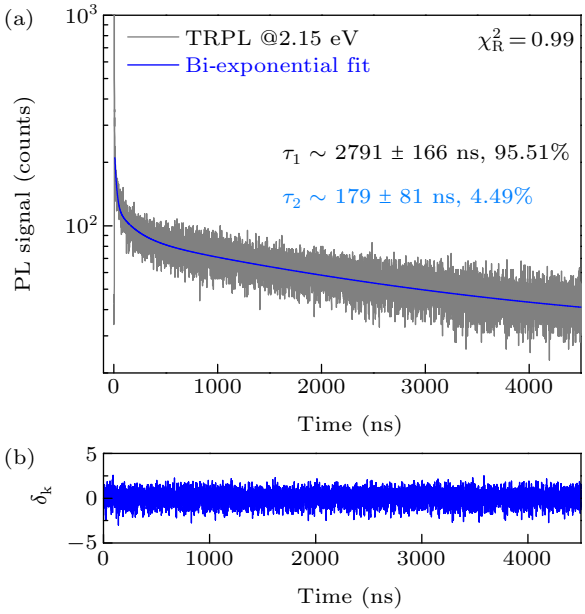


Fig. 5. (a) TRPL traces (grey) recorded at 2.15 eV for $CH_3NH_3PbBr_3$ single crystal along with bi-exponential fit (blue solid line). The yielded two lifetime components and the reduced chi-square are also reported. (b) Standard deviations traced along with bi-exponential fit, showing high-level GOF.

4. Conclusion and outlook

In summary, we developed a room-temperature solution-based crystallization that affords high-quality $CH_3NH_3PbBr_3$ single crystal with atomically flat pristine surfaces. The largely suppressed pristine crystal surface roughness enabled us to observe the unmasked intrinsic luminescence with asymmetric spectral line-shape from the crystal bulk. The agreement between the experimental spectroscopic data and theoretical simulations validates our attribution for the doublet luminescence. Our study confirms that the low-energy PL component with asymmetric spectral line-shape is only attributable to the intrinsic bulk emission from the band-edge states, while the high-energy PL component is attributable to surface-specific emission by excitons. Coexistence of excitons and e–h plasmas were indicated by plausible spectroscopic features. Further efforts aimed at revealing more in-depth intrinsic material physics based on high-quality single-crystal material platform are strongly encouraged.

Acknowledgment

Project supported by the National Natural Science Foundation of China (Grant No. 51872038).

References

[1] Green M A, Ho-Baillie A and Snaith H J 2014 *Nat. Photonics* **8** 506
[2] Correa-Baena J P, Saliba M, Buonassisi T, Grätzel M, Abate A, Tress W and Hagfeldt A 2017 *Science* **358** 739
[3] Yoo J J, Seo G, Chua M R, Park T G, Lu Y, Rotermund F, Kim Y K, Moon C S, Jeon N J, Correa-Baena J P, Bulovic V, Shin S S, Bawendi M G and Seo J 2021 *Nature* **590** 587
[4] Era M, Morimoto S, Tsutsui T and Saito S 1994 *Appl. Phys. Lett.* **65** 676
[5] Hattori T, Taira T, Era M, Tsutsui T and Saito S 1996 *Chem. Phys. Lett.* **254** 103
[6] Kojima A, Teshima K, Shirai Y and Miyasaka T 2009 *J. Am. Chem. Soc.* **131** 6050
[7] Im J H, Lee C R, Lee J W, Park S W and Park N G 2011 *Nanoscale* **3** 4088
[8] Kim H S, Lee C R, Im J H, Lee K B, Moehl T, Marchioro A, Moon S J, Humphry-Baker R, Yum J H, Moser J E, Grätzel M and Park N G 2012 *Sci. Rep.* **2** 591
[9] Lee M M, Teuscher J, Miyasaka T, Murakami T N and Snaith H J 2012 *Science* **338** 643
[10] Rong Y, Hu Y, Mei A, Tan H, Saidaminov M I, Seok S I, McGehee M D, Sargent E H and Han H 2018 *Science* **361** eaat8235
[11] Deschler F, Price M, Pathak S, Klintberg L E, Jarausch D D, Higler R, Huttner S, Leijtens T, Stranks S D, Snaith H J, Atature M, Phillips R T and Friend R H 2014 *J. Phys. Chem. Lett.* **5** 1421
[12] Xing G, Mathews N, Lim S S, Yantara N, Liu X, Sabba D, Grätzel M, Mhaisalkar S and Sum T C 2014 *Nat. Mater.* **13** 476
[13] Cao Y, Wang N, Tian H, Guo J, Wei Y, Chen H, Miao Y, Zou W, Pan K, He Y, Cao H, Ke Y, Xu M, Wang Y, Yang M, Du K, Fu Z, Kong D, Dai D, Jin Y, Li G, Li H, Peng Q, Wang J and Huang W 2018 *Nature* **562** 249
[14] Lin K, Xing J, Quan L N, de Arquer F P G, Gong X, Lu J, Xie L, Zhao W, Zhang D, Yan C, Li W, Liu X, Lu Y, Kirman J, Sargent E H, Xiong Q and Wei Z 2018 *Nature* **562** 245
[15] Dou L, Yang Y M, You J, Hong Z, Chang W H, Li G and Yang Y 2014 *Nat. Commun.* **5** 5404
[16] Lin Q, Armin A, Lyons D M, Burn P L and Meredith P 2015 *Adv. Mater.* **27** 2060
[17] Wei H, Fang Y, Mulligan P, Chuirazzi W, Fang H, Wang C, Ecker B R, Gao Y, Loi M A, Cao L and Huang J 2016 *Nat. Photonics* **10** 333
[18] Shrestha S, Fischer R, Matt G J, Feldner P, Michel T, Osvet A, Levchuk I, Merle B, Golkar S, Chen H, Tedde S F, Schmidt O, Hock R, Rührig M, Göken M, Heiss W, Anton G and Brabec C J 2017 *Nat. Photonics* **11** 436
[19] Nie W, Tsai H, Asadpour R, Blancon J C, Neukirch A J, Gupta G, Crochet J J, Chhowalla M, Tretiak S, Alam M A, Wang H L and Mohite A D 2015 *Science* **347** 522
[20] Wang N, Cheng L, Ge R, Zhang S, Miao Y, Zou W, Yi C, Sun Y, Cao Y, Yang R, Wei Y, Guo Q, Ke Y, Yu M, Jin Y, Liu Y, Ding Q, Di D, Yang L, Xing G, Tian H, Jin C, Gao F, Friend R H, Wang J and Huang W 2016 *Nat. Photonics* **10** 699
[21] Tan H, Jain A, Voznyy O, Lan X, de Arquer F P G, Fan J Z, Quintero-Bermudez R, Yuan M, Zhang B, Zhao Y, Fan F, Li P, Quan L N, Zhao Y, Lu Z H, Yang Z, Hoogland S and Sargent E H 2017 *Science* **355** 722
[22] Wang Y, Li X, Nalla V, Zeng H and Sun H 2017 *Adv. Funct. Mater.* **27** 1605088
[23] Shi D, Adinolfi V, Comin R, Yuan M, Alarousu E, Buin A, Chen Y, Hoogland S, Rothenberger A, Katsiev K, Losovyj Y, Zhang X, Dowben P A, Mohammed O F, Sargent E H and Bakr O M 2015 *Science* **347** 519
[24] Dong Q, Fang Y, Shao Y, Mulligan P, Qiu J, Cao L and Huang J 2015 *Science* **347** 967
[25] Aristidou N, Eames C, Sanchez-Molina I, Bu X, Kosco J, Islam M S and Haque S A 2017 *Nat. Commun.* **8** 15218
[26] Jiang Q, Zhao Y, Zhang X, Yang X, Chen Y, Chu Z, Ye Q, Li X, Yin Z and You J 2019 *Nat. Photonics* **13** 460
[27] Volk S, Yazdani N, Yarema O, Yarema M and Wood V 2020 *ACS Appl. Electron. Mater.* **2** 398
[28] Chen C X, Wang J, Gao M and Shi D 2020 *Cryst. Growth Des.* **21** 45
[29] Fang Y, Dong Q, Shao Y, Yuan Y and Huang J 2015 *Nat. Photonics* **9** 679
[30] Liu Y, Yang Z, Cui D, Ren X, Sun J, Liu X, Zhang J, Wei Q, Fan H, Yu F, Zhang X, Zhao C and Liu S F 2015 *Adv. Mater.* **27** 5176

[31] Comin R, Walters G, Thibau E S, Voznyy O, Lu Z H and Sargent E H 2015 *J. Mater. Chem. C* **3** 8839
[32] Abdi-Jalebi M, Andaji-Garmaroudi Z, Cacovich S, Stavrakas C, Philippe B, Richter J M, Alsari M, Booker E P, Hutter E M, Pearson A J, Lilliu S, Savenije T J, Rensmo H, Divitini G, Ducati C, Friend R H and Stranks S D 2018 *Nature* **555** 497
[33] She X J, Chen C, Divitini G, Zhao B, Li Y, Wang J, Orri J F, Cui L, Xu W, Peng J, Wang S, Sadhanala A and Sirringhaus H 2020 *Nat. Electron.* **3** 694
[34] Yamada T, Yamada Y, Nakaike Y, Wakamiya A and Kanemitsu Y 2017 *Phys. Rev. Appl.* **7** 014001
[35] van Roosbroeck W and Shockley W 1954 *Phys. Rev.* **94** 1558
[36] Yamada T, Aharen T and Kanemitsu Y 2018 *Phys. Rev. Lett.* **120** 057404
[37] Saba M, Cadelano M, Marongiu D, Chen F, Sarritzu V, Sestu N, Figus C, Aresti M, Piras R, Lehmann A G, Cannas C, Musinu A, Quochi F, Mura A and Bongiovanni G 2014 *Nat. Commun.* **5** 5049
[38] Davies C L, Filip M R, Patel J B, Crothers T W, Verdi C, Wright A D, Milot R L, Giustino F, Johnston M B and Herz L M 2018 *Nat. Commun.* **9** 293
[39] D'Innocenzo V, Grancini G, Alcocer M J, Kandada A R, Stranks S D, Lee M M, Lanzani G, Snaith H J and Petrozza A 2014 *Nat. Commun.* **5** 3586